J. Membrane Biol. 189, 201–212 (2002)
DOI: 10.1007/s00232-002-1014-8

The Journal of
Membrane
Biology

Analysis of the K^+ Current Profile of Mature Rat Oligodendrocytes in situ

K. Gipson[1], **A. Bordey**[1,2]
[1]Interdepartmental Neuroscience Graduate Program, [2]Department of Neurosurgery, Yale University School of Medicine, 333 Cedar St. New Haven, CT 06520-8082, USA

Received: 9 March 2002/Revised: 19 June 2002

Abstract. Previous studies have reported that mature oligodendrocytes (OLGs) in vitro display various voltage-dependent K^+ currents while in situ OLGs show only voltage-independent K^+ currents. Given this discrepancy and the lack of information on myelinating OLG ion channel expression in situ, we characterized mature OLG currents in myelinating corpus callosum slices from 17 to 36-day old rats. OLGs were recorded in cell-attached and whole-cell patch-clamp configurations, displayed morphology typical of mature OLGs, and stained positive for myelin basic protein. OLGs displayed large voltage-independent currents that decayed during the voltage pulse and small voltage-activated outward currents. The latter were blocked by TEA, activated between −40 and −50 mV, and decayed slowly. The former were composed of large voltage-independent, time-dependent Ba^{2+} (1 mM)-sensitive currents, and voltage-dependent Cs^+ (5 mM) and Ba^{2+} (100 μM)-sensitive currents that reversed near the K^+ equilibrium potential and inactivated at hyperpolarized potentials, identifying them as inwardly rectifying K^+ currents. Inwardly rectifying single-channel K^+ currents could be recorded in the cell-attached configuration. The estimated single-channel slope conductance was 30 pS. The steady-state open probability was voltage-dependent and declined from 0.9 to 0.5 between −80 and −150 mV. Overall, mature OLGs in situ possess time- and also voltage-dependent K^+ currents, which may facilitate clearance of K^+ released during axonal firing.

Key words: Patch clamp — Glial cells — Slices — Inwardly rectifying K^+ channels — Delayed rectifier K^+ channels — Node of Ranvier — K^+ buffering

Correspondence to: A. Bordey; email: angelique.bordey@yale.edu

Introduction

Oligodendrocytes (OLGs) form the myelin around CNS axons that allows proper saltatory conduction of action potentials. Beyond their role as insulators, mature OLGs have been suggested to participate in K^+ buffering along axons (Berger, Schnitzer & Kettenmann, 1991; Chvatal et al., 1999). In astrocytes, K^+ buffering is performed by K^+ channels that are open at rest, the inwardly rectifying K^+ channels (K_{IR}) (Newman, Frambach & Odette, 1984; Newman, 1993), and by spatial buffering through the glial syncitium (Orkand, Nicholls & Kuffler, 1966). Like astrocytes, OLGs possess various ion channels, the expression of which depends on the stage of OLG differentiation (Soliven et al., 1988; Sontheimer et al., 1989; Attali et al., 1997) and whether OLGs are studied in vitro (Barres, Chun & Corey, 1988; Soliven et al., 1989; Soliven & Wang, 1995; Williamson, Compston & Randall, 1997; Hida, Takeda & Soliven, 1998) or in situ (Berger et al., 1991; Chvatal et al., 1999). In vitro differentiated OLGs express K_{IR} channels and voltage-dependent outward K^+ channels. However, in situ differentiated OLGs in postnatal day (P) 10–13 mice and P10–P20 rats are thought to have only passive, decaying currents. These voltage-independent channels have been suggested to allow the flux of K^+ across the OLG membrane and aid extracellular K^+ buffering. A recent study in situ demonstrated the presence of mRNA and membrane expression of one subunit of K_{IR} channels in presumed OLGs from adult rats (Poopalasundaram et al., 2000). This result suggests the presence of possibly functional K_{IR} channels in OLGs in situ as observed in vitro. In addition, K_{IR} channels have been shown to be necessary for myelin maintenance (Soliven, Takeda & Szuchet, 1994).

Given the discrepancy between in vitro and in situ studies of OLG current profiles and the importance of K^+ channels in K^+ buffering and myelination

(Soliven et al., 1989; Neusch et al., 2000; Sutor et al., 2000), we set out to investigate the current identity of mature, myelinating OLGs in situ. To date, no comprehensive pharmacological characterization of currents in myelinating OLGs in situ has been performed. The corpus callosum slice preparation is commonly used to study OLG properties and this region displays demyelination plaques in experimental allergic encephalomyelitis animals (Petry et al., 2000) and multiple sclerosis patients (Simon et al., 1986). It is crucial to know the pattern of ion channel expression since this feature is important for understanding OLG function in the normal CNS and following demyelination. In our experiments, patch-clamp recordings were made from mature OLGs in corpus callosum slices from P17 to 36 rats after the beginning of myelination at P14–15 (Sturrock, 1980). Mature OLGs were identified by their morphology and by immunostaining for myelin basic protein (MBP). Recorded OLGs displayed TEA-sensitive voltage-activated outward K^+ currents, voltage-dependent Cs^+ and Ba^{2+} (100 μM)-sensitive K^+ currents, and Ba^{2+} (1 mM)-sensitive voltage-independent currents.

Materials and Methods

Slice Preparation

Slices including the corpus callosum were prepared as previously described (Berger et al., 1991). Briefly, 17- to 36-day old Sprague Dawley rats were anesthetized using pentobarbital (50 mg/kg) and decapitated. The brain was hemisected, quickly removed and chilled (0–4°C) in 95% O_2/5% CO_2 saturated artificial cerebrospinal fluid (ACSF) containing (in mM): NaCl 125; KCl 3; $CaCl_2$ 2; $MgCl_2$ 2; $NaHCO_3$ 25; glucose 10. The tissue of interest was glued (cyanoacrylate glue) to the stage of a Vibratome and slices (250 μm thick) were cut in cold oxygenated ACSF. After a recovery period of at least 1 hour in ACSF, slices were placed in a flow-through chamber, held in position by a nylon mesh glued to a U-shaped platinum wire and continuously superfused with oxygenated ACSF at room temperature. The chamber was mounted on the stage of an upright microscope (Olympus BX50WI) equipped with a 60× water immersion objective and infra-red optics.

Whole-Cell and Single-Channel Recordings

Whole-cell patch-clamp recordings were obtained as previously described for hippocampal and corpus callosum slices (Berger et al., 1991; Bordey & Sontheimer, 1997). Patch pipettes were pulled from thin-walled borosilicate glass (o.d., 1.55 mm; i.d., 1.2 mm, WPI, TW150F-40) on a PP-83 puller (Narishige, Japan). Pipettes had resistances of 4–7 MΩ when filled with the following solutions (in mM): KCl 140 or CsCl 140 or KGluconate 140 when noted; $CaCl_2$ 1.0; $MgCl_2$ 1.0; ethylene glycol-bis (-aminoethyl ether)-N,N,N′,N′-tetraacetic acid (EGTA) 10; HEPES 10; Na_2ATP 4, pH adjusted to 7.2 with NaOH. The osmolarity of the intracellular and extracellular solutions were 295–300 and 305–310 mOsm, respectively. The osmolarity of all solutions was measured with a vapor pressure osmometer 5500 (Wescor) and was adjusted by addition of water (decreasing osmolarity) or sucrose (increasing osmolarity). To label cells for later morphological identification and antigenic identification, 0.1% Lucifer Yellow (LY, dilithium salt) was added to the pipette solution. Whole-cell and cell-attached recordings were performed using an Axopatch-200B amplifier (Axon Instruments). Current signals were low-pass filtered at 1 kHz and 3–5 kHz for single-channel and whole-cell recordings, respectively, and digitized on-line at 5–20 kHz using a Digidata 1320 digitizing board (Axon Instruments) interfaced with an IBM-compatible computer system. Data acquisition, storage and analysis were done using PClamp version 8 (Axon Instruments). For all measurements, capacitance compensation and series resistance compensation (60–70%) were used to minimize voltage errors. Settings were determined by compensating the transients of a small (5 mV) 10-msec hyperpolarizing voltage step. The capacitance reading of the amplifier was used as the value for the whole-cell capacitance. Membrane resistance (R_m) was evaluated from the average response to 50 hyperpolarizing (10 mV) current pulses (20 msec). The conductance was calculated using the equation: $G = I/(V-E_K)$ where V is the membrane potential, E_K is the Nernst equilibrium potential for K^+ ($E_K = -96$ mV). Unless indicated otherwise, capacitive and leak conductances were not subtracted. Peak currents were determined using Clampfit (Axon Instruments), and statistical values (mean ± SD, with n being the number of cells tested) were evaluated with a statistical graphing and curve-fitting program (Origin, MicroCal). For single-channel analysis, the analysis routines used PClamp (version 8) to determine the amplitudes and the open and closed times for channel events with threshold for detection set at 50% of a full opening. Peaks of the open and closed current levels were determined by eye, using a cursor. The duration histogram did not include events with duration less than 1 msec. Only data recorded from patches with the activity from only one channel were analyzed. The fraction of time a channel was in the closed or open state was determined by measuring the area under the amplitude histogram for that state and dividing by the total time at a specified holding potential. Currents were binned in intervals of 0.02 to 0.05 pA.

Cell Identification

Images of cells visually chosen for recordings were archived using an LGS frame grabber (Scion Corporation, Maryland) for later (off-line) comparison to LY fills. After recordings, slices were transferred to a fixation medium containing 4% paraformaldehyde in phosphate-buffered saline (PBS). The next day, slices were washed three times in Tris-buffered saline (TBS) 2× for 1 hour, were incubated for 15 min with 1.25% Triton X-100, 5% normal goat serum (NGS, Sigma) in TBS 2× and then were incubated for 1 hour in the blocking solution 0.2% Triton X-100, 5% NGS in TBS. Slices were then incubated for 24 hours at 4°C with the rabbit primary polyclonal antibody to myelin basic protein at 1:50 (AB980, Chemicon) in the blocking solution. Slices were washed three times with TBS for 5 min and incubated with the secondary antibody (goat anti-rabbit IgG), conjugated to Texas Red (dilution 1:200, Vector) for 2 hours at room temperature. Slices were then mounted on glass coverslips with fluorescent mounting medium (Vector) and were viewed on an epifluorescence microscope using standard procedures. For glial fibrillary acidic protein (GFAP) immunostaining, slices were similarly washed in TBS, permeabilized with Triton X-100 and incubated with a Cy3-conjugated antibody against GFAP (Sigma, dilution on 1:500) for 2 hr at room temperature in the same solution as for MBP staining. Slices were then washed in TBS and mounted on coverslips. LY labeling and MBP or GFAP staining were visualized on an Olympus microscope (BX51). Images were captured with a DVC color camera and

printed on an Epson color printer. Some cells were imaged on a confocal scanning laser microscope (Biorad MRC600). High magnification (40×) serial optical sections were taken at consecutive focal levels of 1–2 μm apart. Addition of data from all section series enabled the 3-dimensional morphology of the cell to be represented in a 2-dimensional image. No bleed-through was observed between the Texas Red/Cy3 and FITC fluorescence channels in control experiments.

Chemicals were purchased from Sigma (St. Louis, MO) unless otherwise noted.

Results

Whole-cell recordings were obtained from 63 visually identified oligodendrocytes located in the corpus callosum of 17–36-day-old rats. The approximate location for each cell was documented through a low power fluorescence image after recordings. In KCl- and KGluconate-based intracellular media, recorded cells had a mean resting membrane potential (V_R) of -79.8 ± 4.7 mV (mean ± SD, $n = 53$) and an input resistance (R_m) of 58.4 ± 21.0 MΩ. Because no significant difference for these parameters was observed between the two intracellular media, values were pooled. These values were determined in the first 3 min of whole-cell recording. The remaining 10 cells were recorded in CsCl-based intracellular medium. Cells that exhibited >10% change in series resistance (R_s) and whole-cell membrane capacitance (C_m), indicative of a whole-cell closure, were disregarded. Cells exhibiting a C_m smaller than 30 pF were also disregarded. Recorded cells had a mean C_m of 56.2 ± 24.8 pF ($n = 63$) and a mean R_s of 13.9 ± 4.3 MΩ before applying a 63.3 ± 5.7% compensation.

Cell Morphology and Identification

Infrared optics allowed us to choose oligodendrocytes over astrocytes for recordings. OLG cell bodies were large (20–25 μm long) and were usually elongated (Fig. 1*A*, left panel) or triangular. Once filled with Lucifer Yellow (LY), long parallel processes following the axonal tracts could be observed. Perpendicular processes were observed in 11 of 33 cells, numbered 3 ± 2 per cell, and correlated with visualized axons crossing over the corpus callosum. The mean number and length of the parallel processes were 15.2 ± 3.7 and 132.2 ± 36.0 μm ($n = 35$), respectively. Figure 1*A* illustrates a representative example of a LY-filled cell at 25 days, showing a morphology typical of differentiated OLGs (Remahl & Hilderbrand, 1990; Bjartmar, Hildebrand & Loinder, 1994; Butt et al., 1997). All of the OLGs showing this typical morphology were negative for glial fibrillary acidic protein (GFAP), a marker of astrocytes (Eng, 1985) (Fig. 1*A*, right panel, same field as that of LY-fill). In addition, myelinated fibers in the corpus callosum stained positive for myelin basic protein (MBP) at the age studied (*data not shown*). Occasionally, recorded cells displayed a stellate shape reminiscent of NG2-positive oligodendrocytes (Nishiyama, Chang & Trapp, 1999; Butt et al., 1999; Dawson, Levine & Reynolds, 2000) and did not stain positive for MBP (*data not shown*). These cells had longer processes than astrocytes, which also display a stellate shape (Bordey & Sontheimer, 2000). Neurons were also occasionally recorded in the splenium of the corpus callosum and the cingulum bundle, but were easily identified morphologically and electrophysiologically. Under normal recording conditions, LY coupling was never observed, as previously reported for OLGs in mouse corpus callosum (Berger et al., 1991).

Biophysical and Pharmacological Properties of Whole-cell Currents

Whole-cell currents were activated in voltage-clamped cells by applying ramp protocols from −140 to +100 mV, and hyperpolarizing and depolarizing steps from a holding potential of −70 or −80 mV. Typical ramp-activated currents are illustrated in Fig. 1*A* and correspond to the LY-filled cell displayed on the left. Ramp currents are characterized by large inward currents at hyperpolarized potentials and an almost linear appearance between −80 and +80 mV, with occasionally some apparent voltage-dependence between −25 and +80 mV. 20 mV-increment voltage steps were applied from −160 mV to +60 mV for 400 msec from a holding potential of −80 mV (Fig. 1*B*). Figure 1*B* displays typical current traces from an OLG from a P21 animal. These traces illustrate the presence of large transient currents followed by smaller inward and outward currents. At hyperpolarized potentials, a small inactivation of the inward currents can be observed and will be further described below. Figure 1*C* displays the current-voltage (*I-V*) relationships of the peak (empty squares) and steady-state (filled squares) currents for the traces shown in Fig. 1*B*. The *I-V* curves of the peak currents are strictly linear, illustrating the voltage-independence of the transient currents. The *I-V* curves of the steady-state currents illustrate the inactivation at hyperpolarizing potentials and the voltage-dependence at potentials more positive than −50 mV, as observed by deviation from the straight line (dashed line). This *I-V* curve gives a reversal potential (E_{REV}) of the steady-state currents of −80 mV (mean of -75.9 ± 3.8 mV, $n = 20$), showing a major contribution of K^+ channels to these currents (Nernst equilibrium potential for K^+ equals −96 mV).

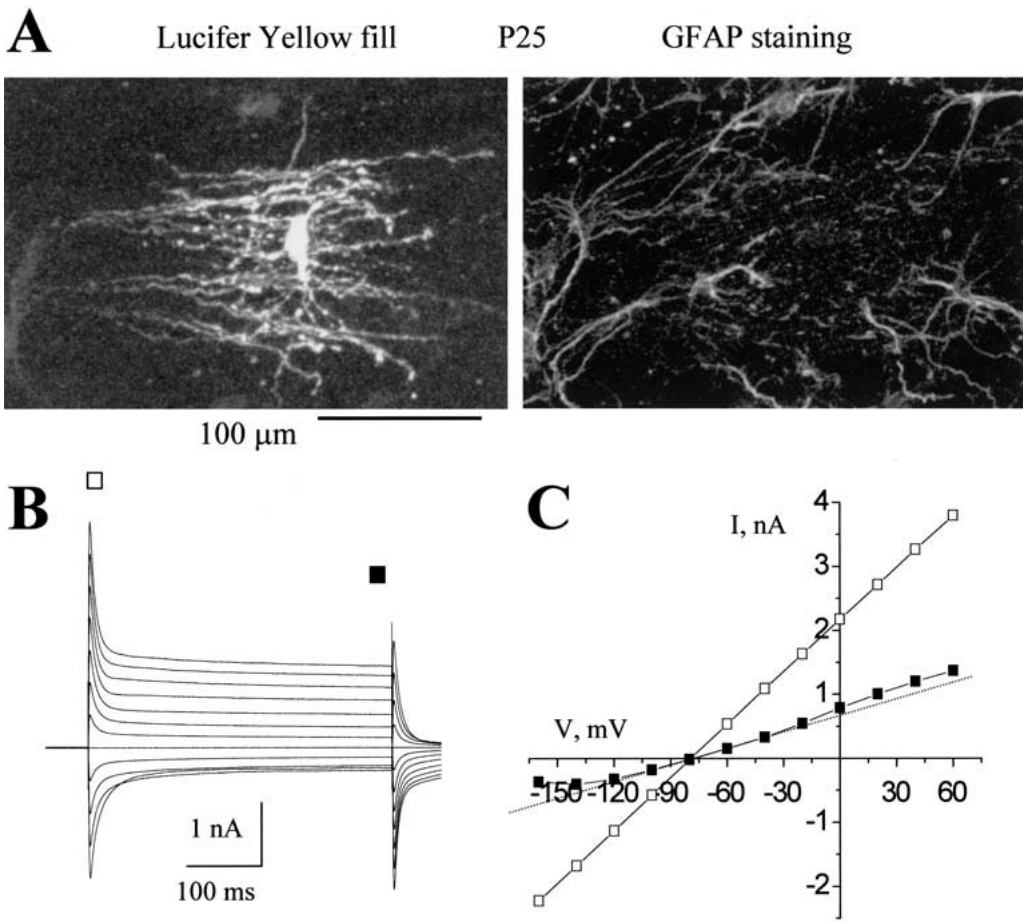

Fig. 1. OLG morphology. (*A*) A Lucifer Yellow-filled OLG (left panel) and anti-GFAP antibody labeling (right panel) of the same field. The recorded OLG stained negative for GFAP and displays longitudinally orientated processes. The images in (*A*) are confocal reconstructions from 16 sections. (*B*) Whole-cell current traces from a P21 oligodendrocyte. Voltage steps were applied from -160 to +60 mV for 400 msec from a holding potential of -80 mV. (*C*) *I-V* curves of the peak transient currents (*empty squares*) and steady-state currents (*filled squares*) of the traces in (*B*).

TEA-Sensitivity of Whole-Cell Outward Currents Reveals the Presence of Delayed Rectifying Outward K^+ currents

Figure 2*A* shows that TEA (40 mM) ($n = 15$) blocked an outward voltage-dependent current (control: dashed lines; TEA: solid lines). Such voltage-dependent currents were detectable in 78% of the records. To better characterize TEA-sensitive outward currents, OLGs were held at −70 mV and depolarizing voltage steps were applied following a 200-msec conditioning pre-pulse to −50 mV. Voltage-dependent outward currents that showed delayed activation and slow inactivation were observed (Fig. 2*B*). Neither the amplitude nor the kinetics of these currents was affected by the application of a hyperpolarizing pre-pulse potential (−110 mV; *data not shown*), suggesting that transient, A-type currents are absent in mature OLGs. Bath application of TEA (20 mM) reversibly and selectively reduced the sustained currents without affecting the transient capacitive currents (Fig. 2*Bb* and inset; squares and circles, respectively). Point-by-point subtraction of the sustained currents in the presence (Fig. 2*Bb*) and absence of TEA (Fig. 2*Ba*) isolated TEA-sensitive currents that resembled delayed rectifying K^+ currents observed in other cell types (Fig. 2*C*). The *I-V* relationship of TEA-sensitive currents suggests an activation threshold between −50 and −40 mV (Fig. 2*D*, $n = 6$). 40 mM TEA reversibly and completely blocked outward K^+ currents (*data not shown*). 40-mM TEA-sensitive currents measured at 20 mV averaged 7.6 ± 2.7 pA/pF ($n = 15$). The mean density of conductance (conductance divided by the membrane capacitance) was 65.6 ± 23.6 pS/pF, which represents an estimation of the delayed rectifying K^+ conductance in OLGs in our recording conditions. Current amplitudes are given as a density of currents, which are the currents divided by the cell capacitance to eliminate cell-to-cell variability. Whole-cell cur-

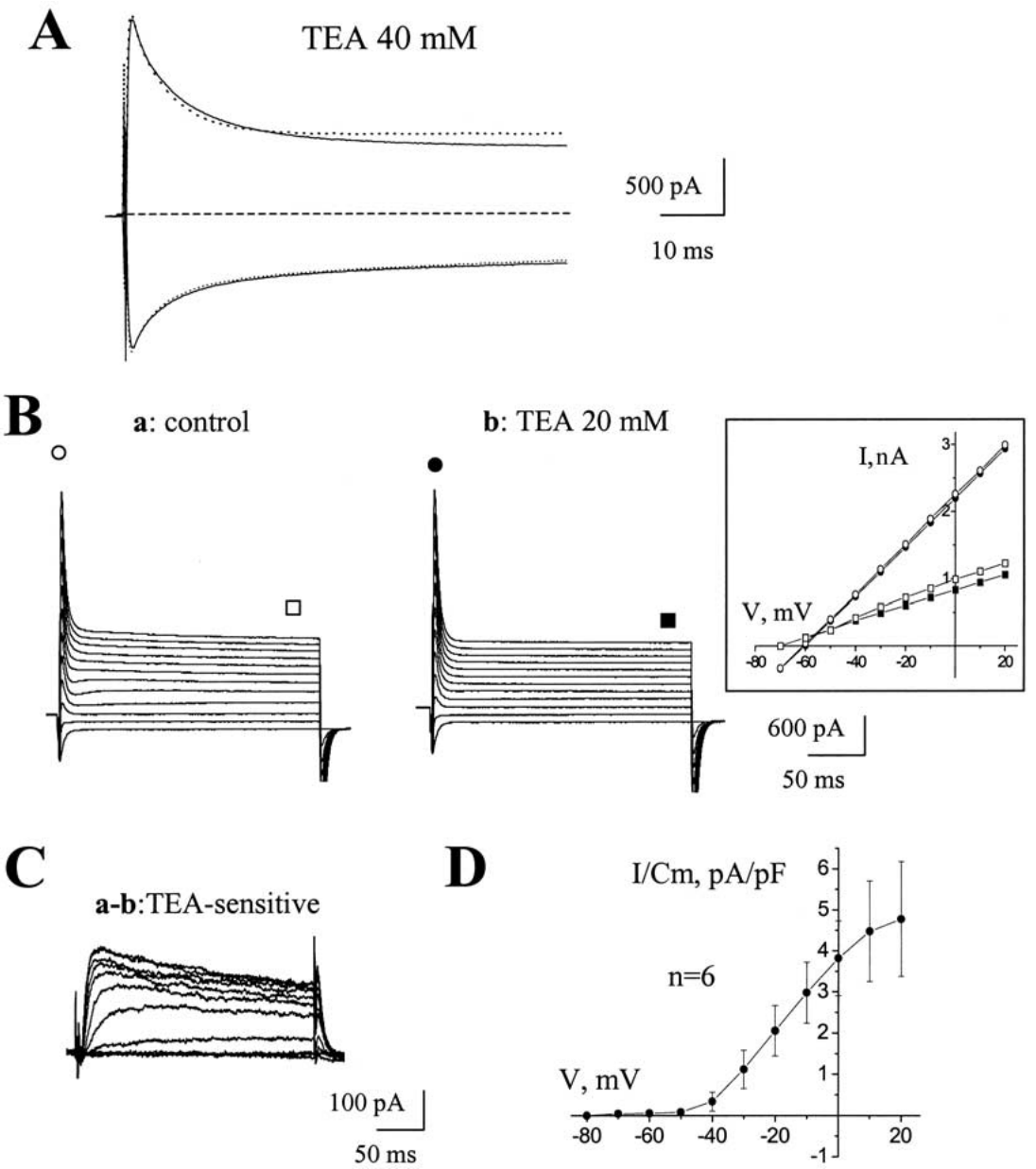

Fig. 2. TEA-sensitive outward K^+ currents. (*A*) Control current traces (*dotted lines*) and traces in the presence of 40 mM TEA (*solid lines*) for voltage steps to −160 and +20 mV from a holding potential of −80 mV. (*B*) Voltage steps from −70 mV to 20 mV from a holding potential of −70 mV evoked voltage-dependent sustained outward currents (*Ba*) that are reduced by application of TEA (20 mM) (*Bb*). *Inset: I-V* curves of the peak transient currents (*circles*) and of the voltage-dependent outward currents (*squares*) in control (*empty symbols*) and in the presence of TEA (*filled symbols*). (*C*) Point-by-point subtraction of the currents in TEA (*Bb*) from the control currents (*Ba*) resulting in the isolation of the TEA-sensitive currents. (*D*) *I-V* curve of the TEA-sensitive current displayed in (*C*).

rents were further characterized based on their pharmacological properties. Application of TEA (20 mM) did not significantly alter the input resistance and V_R of the cells (V_R equal −78.6 ± 3.2 mV in the presence of TEA, $n = 11$) nor did it affect E_{REV} of the steady-state currents (−76.0 ± 3.8 mV in control and −75.8 ± 3.7 mV in the presence of TEA, $n = 11$).

Cs^+- and Ba^{2+}-Sensitivity of Whole-Cell Inward Currents Reveals the Presence of Inwardly Rectifying K^+ Currents

Bath application of Cs^+ (5 mM + TEA 40 mM) ($n = 15$) reversibly blocked inward currents (control: dashed lines; Cs^+ + TEA: solid lines) without af-

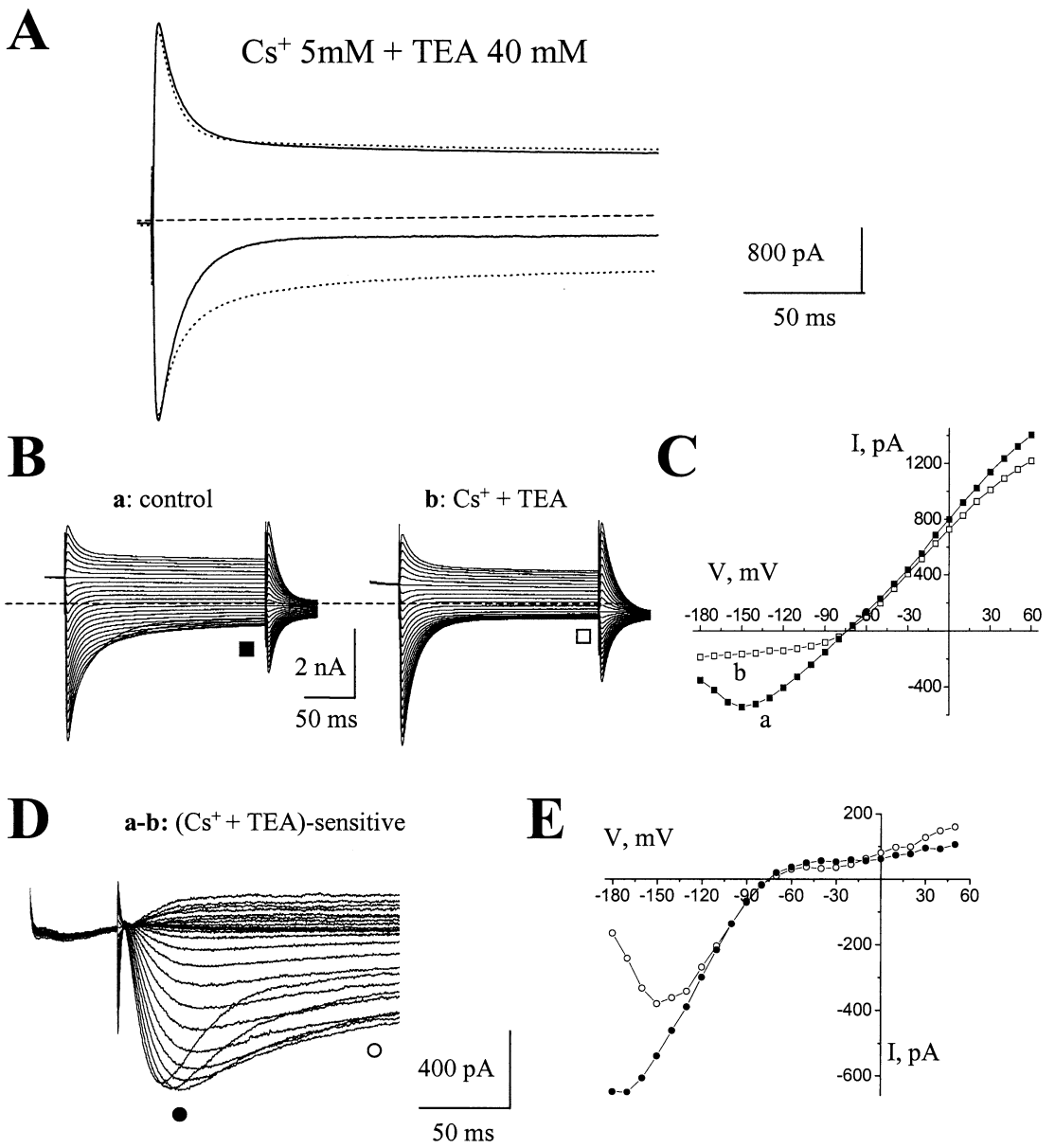

Fig. 3. Cs^+-sensitive inward K^+ currents. (*A*) Control current traces (*dotted lines*) and traces in the presence of 5 mM Cs^+ and 20 mM TEA (*solid lines*) for voltage steps to −160 and +20 mV from a holding potential of −80 mV. (*B*) Inward currents were activated by depolarizing the cell to 0 mV for 100 msec before giving hyperpolarizing voltage steps from −180 to +50 mV. Currents recorded in control (*a*) and in the presence of 5 mM Cs^+ and 40 mM TEA (*b*). (*C*) *I-V* curves of the currents in control (*filled squares*) and in the presence of TEA/Cs^+ (*empty squares*). (*D*) Subtracted (Cs^+ + TEA) -sensitive currents. (*E*) *I-V* curves of the peak (*filled circles*) and steady-state (*empty circles*) (Cs^+ + TEA) -sensitive inward currents.

fecting the transient components of inward currents (Fig. 3*A*). 100 μM Ba^{2+} ($n = 3$) had effects similar to Cs^+ (*data not shown*). To further characterize these Cs^+-sensitive inward currents, whole-cell recordings were obtained in which the membrane was stepped from a pre-pulse potential of 0 mV to potentials ranging from −180 to +50 mV (Fig. 3*B*). This protocol activated large inward currents. The *I-V* curve of the currents measured at the end of the pulse reveal that these currents reverse direction at −75 mV, suggesting the activation of K^+ conductances (Fig. 3*C*). Both Cs^+ (5 mM + TEA 40 mM, Fig. 3*Bb*) and Ba^{2+} (100 μM, *data not shown*) blocked inward currents that averaged −11.4 ± 5.2 pA/pF ($n = 15$) and −12.2 ± 2.8 pA/pF ($n = 3$), respectively, when measured at the peak of the current at −160 mV. Point-by-point subtractions of the currents in the presence of 5 mM Cs^+ (traces *b*) from those in control (traces *a*) isolated Cs^+-sensitive currents (Fig. 3*D*). At potentials more negative than −130 mV, Cs^+-

sensitive currents show a time- and voltage-dependent inactivation that is characteristic of inwardly rectifying K^+ currents, including those observed in cultured OLGs (Soliven et al., 1988; Hertz et al., 1990; Gaillard & Bossu, 1995). *I-V* curves for the peak (filled symbols) and steady-state (empty symbols) current components show the inactivation at hyperpolarized potentials (Fig. 3*E*). Steady-state current *I-V* curves gave E_{REV} of -81.2 ± 1.8 mV ($n = 15$) for Cs^+- and Ba^{2+}-sensitive currents. Cs^+ or Ba^{2+} induced positive shifts in V_R of ~13 mV (-82.3 ± 2.9 in control and -69.3 ± 4.1 mV in the presence of Cs^+ or Ba^{2+}, $n = 15$, $p < 0.001$; data were pooled for Cs^+ and Ba^{2+}). Consistent with this value, the mean V_R of OLGs recorded with intracellular CsCl and extracellular TEA (40 mM) was -49.6 ± 6.6 mV ($n = 10$). Extracellular TEA + Cs^+ also significantly shifted E_{REV} of the steady-state currents to more depolarized potentials (-75.8 ± 4.0 mV in control and -69.7 ± 6.2 mV with Cs^+ or Ba^{2+}, $n = 15$, $p < 0.02$).

Ba^{2+} (1 mM)-Sensitivity of Whole-cell Currents Reveals the Presence of Voltage-independent Currents

Ba^{2+} at 1 mM blocked both inward and outward components of the whole-cell currents ($n = 5$) (control: dashed lines; Ba^{2+}: solid lines) without affecting the amplitude of the transient currents (Fig. 4*A*). To better characterize Ba^{2+}-sensitive outward currents, OLGs were depolarized from -160 to $+50$ mV from a holding potential of -80 mV in control (Fig. 4*Ba*) and in the presence of 1 mM Ba^{2+} (Fig. 4*Bb*). Ba^{2+} completely blocked inward currents and reduced outward currents (Fig. 4*A* and *C*, filled symbols) without affecting the transient current component (Fig. 4*A* and *C*, open symbols). Voltage-dependent outward currents are revealed in the presence of Ba^{2+} (Fig. 4*B*, traces *b*). Point-by-point subtractions of the currents in the presence of 1 mM Ba^{2+} (traces *b*) from those in control (traces *a*) isolated Ba^{2+}-sensitive voltage-dependent currents that show an inward rectification of the peak currents and inactivation at hyperpolarized potentials that are reminiscent of inwardly rectifying K^+ currents (Fig. 4*D* and *E*). Ba^{2+} induced positive shifts in V_R of ~23 mV (-81.7 ± 5.5 mV in control and -58.3 ± 1.5 mV with Ba^{2+}, $n = 5$, $p < 0.001$) and significantly shifted E_{REV} of the steady-state currents to more depolarized potentials (-68.7 ± 4.2 mV with Ba^{2+}, $n = 51$). This shift is likely due to blockade of both inwardly rectifying K^+ currents and steady-state passive currents.

None of the above pharmacological treatments significantly affected the peak amplitude of the transient components of the whole-cell currents. Similarly, when recorded with a CsCl-based intracellular solution and extracellular TEA (40 mM), records display large transient currents at the onset of the voltage steps. These transient components of the currents are likely uncompensated capacitive currents due to the extensive myelin membrane that behaves like a capacitor. In fact we found a good correlation between the amplitudes of the transient currents measured at -140 mV and $+20$ mV and the cell capacitances ($r = 0.73$ and 0.69, respectively) (*data not shown*). No fast inward currents could be detected when OLGs were depolarized from -70 to $+60$ mV following a pre-pulse to -110 mV, commonly used to activate Na^+ currents, Similarly, TTX did not block any inward currents in OLGs (*data not shown*).

Single-channel Properties of Inwardly Rectifying K^+ Currents

Figure 5*A* shows an example of single-channel activity in the cell-attached configuration at various holding potentials from an OLG recorded with a pipette solution containing 140 mM KGluconate. Current fluctuations increased in amplitude as holding potentials became more negative, and did not reverse at positive potentials, demonstrating that the channel rectifies inwardly. Inward single-channel currents were observed in 75% of the recorded cells, as regularly tested by applying a ramp protocol from -140 to $+140$ mV (applied potential in the patch pipette, V_{PIP}). In only one out of 40 cells we observed more than one active channel in a patch, which indicates a relatively low channel density on the cell soma. The amplitude histogram in the inset of Fig. 5*B* illustrates the presence of only one channel per patch. Outward single-channel currents were never observed in membrane patches, suggesting that such channels are not present on the cell soma (Fig. 5*A* at +30 mV). Single-channel conductance (γ) was determined by measuring the slope of the linear portion of the single-channel *I-V* relationship (Fig. 5*B*) and averaged 31.8 ± 2.4 pS ($n = 4$, including two OLGs recorded with 140 mM KGluconate and two with 140 mM KCl). An accurate way to measure E_{REV} in this case is to apply a voltage ramp and determine the voltage at which the open and closed current levels intersect (Fig. 5*C*). When E_{REV} was measured in this way, it was found to be close to E_K in all the tested cells ($n = 22$). E_K was between 3–7 mV for each patch (assuming an intracellular K^+ concentration of 105–125 mM; Ballanyi, 1995; Stys et al., 1997). An example of single-channel currents recorded with a KGluconate pipette solution measured in response to a ramp stimulus is given in Fig. 5*C*. To determine whether single channels inactivate, we recorded currents in response to voltage steps in the cell-attached con-

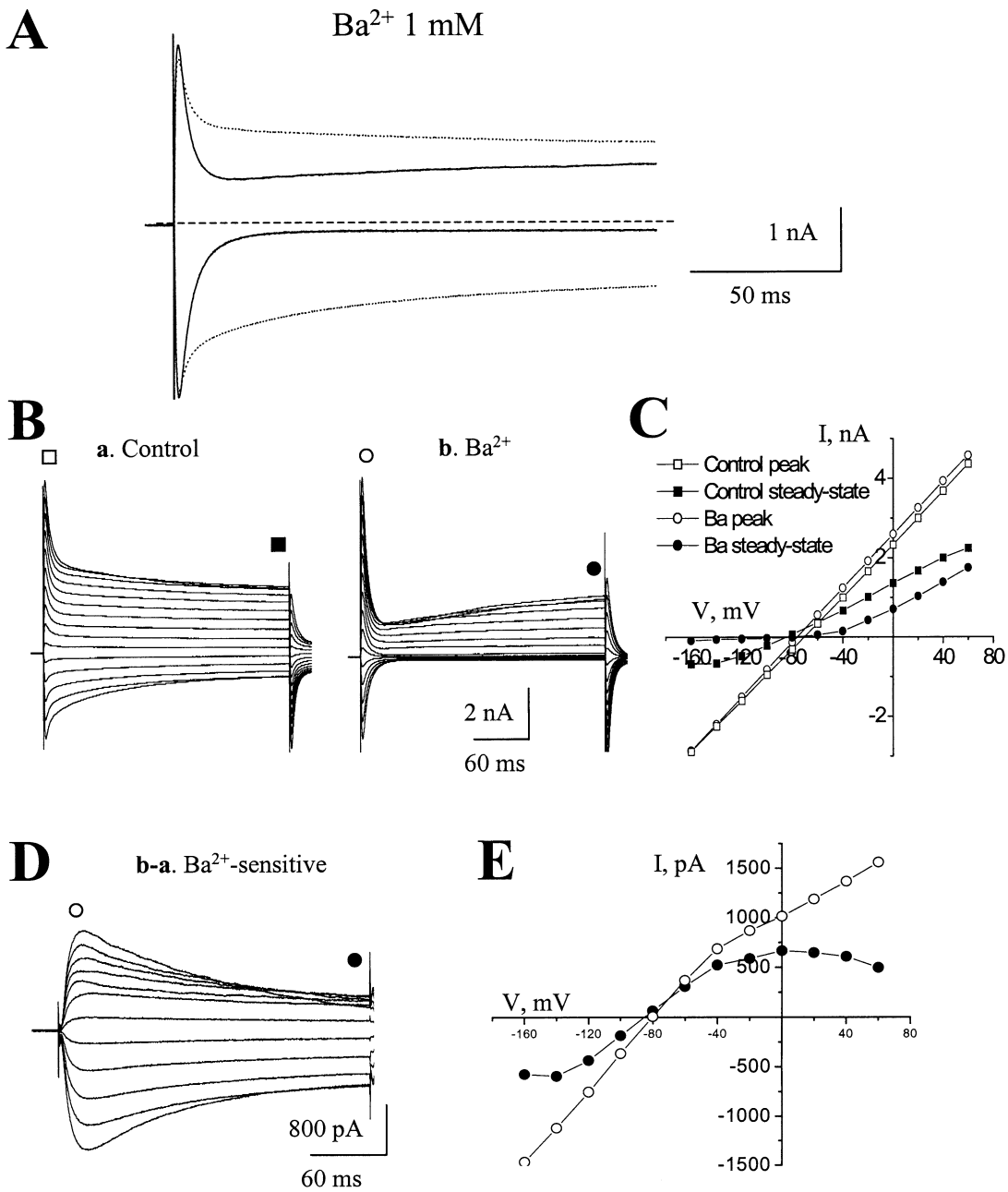

Fig. 4. 1-mM Ba^{2+}-sensitive voltage-independent K^+ currents. (*A*) Control current traces (*dotted lines*) and traces in the presence of 1 mM Ba^{2+} (*solid lines*) for voltage steps to −160 and +20 mV from a holding potential of −80 mV. (*B*) Currents were activated by applying voltage steps from −160 to +60 mV for 300 msec from a holding potential of −80 mV. Currents recorded in control (*a*) and in the presence of 1 mM Ba^{2+} (*b*). (*C*) *I-V* curves of the peak (*empty symbols*) and steady-state (*filled symbols*) currents in control (*squares*) and in the presence of Ba^{2+} (*circles*). (*D*) Subtracted Ba^{2+}-sensitive currents. (*E*) *I-V* curves of the peak (*empty circles*) and steady-state (*filled circles*) Ba^{2+}-sensitive inward and outward currents.

figuration (Fig. 6). OLG patches were recorded at a V_{PIP} of 0 mV and stepped to more positive pipette potentials (equivalent to hyperpolarized patch potentials V_P). Upon stepping to more hyperpolarized patch potentials (−160 versus −90 mV, Fig. 6*A* right and left panels, respectively) the channel did not strongly inactivate during the recording, although the channel was more frequently in the closed state. When many sweeps were averaged, the resulting current trace showed little inactivation at −160 mV and no inactivation at −90 mV, as illustrated in Fig. 6*A* and *B*, respectively (bottom traces). The steady-state open probability of the inwardly rectifying channel declines as potentials become more hyperpolarized. The dependence of open probability on V_P is shown in Fig. 6*B*. The data were fitted by a

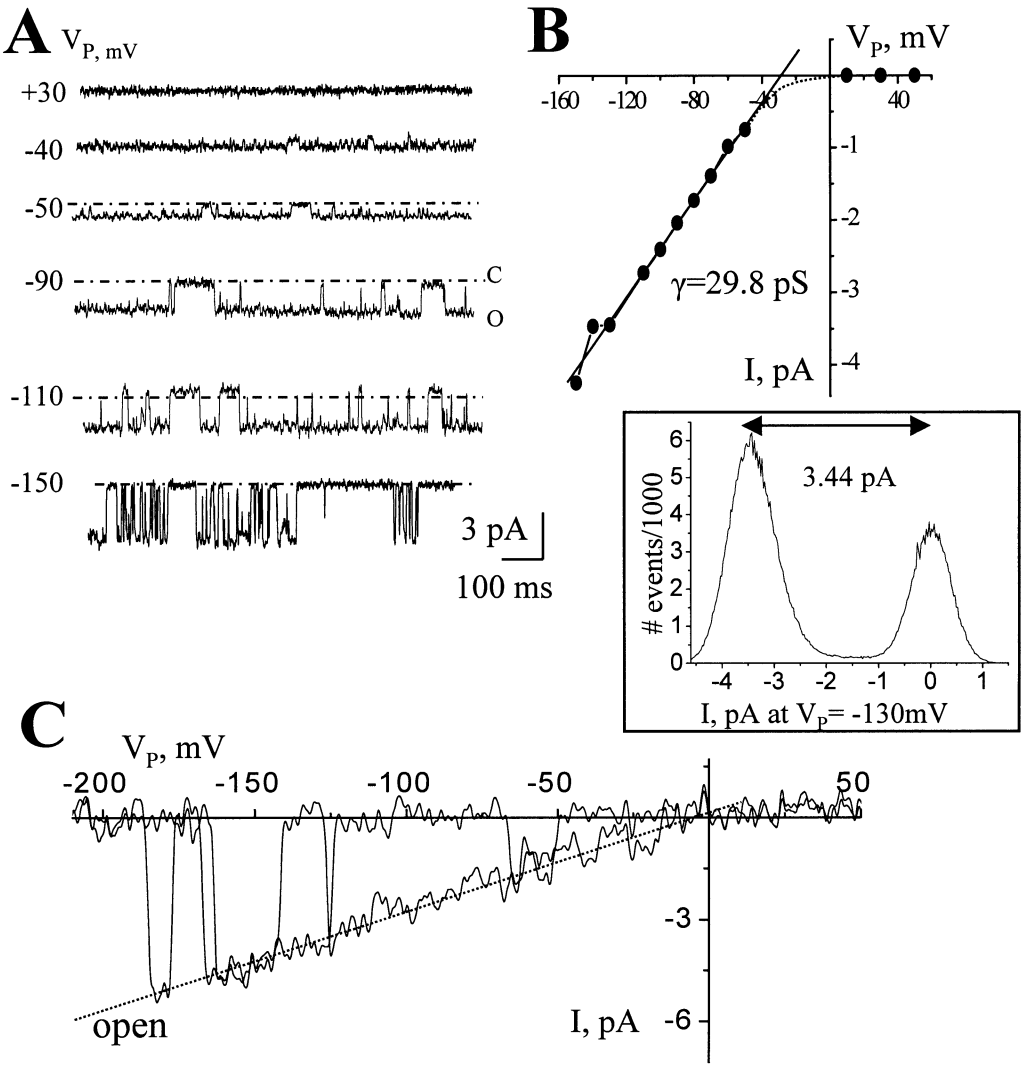

Fig. 5. Single-channel conductance (γ). (*A*) Cell-attached patch recordings of single-channel currents at various holding potentials from a P19 OLG. The potentials on the left represent the potentials across the patch of membrane under the pipette (V_P) given as $V_R - V_{PIP}$, V_{PIP} being the potential applied to the patch pipette. V_R was -75 mV in this cell. O and C represent open and closed states, respectively. (*B*) Single-channel *I-V* relationship for the cell record shown in (*A*). The solid line is a least-squares fit of the linear portion of the data and gave γ of 29.8 pS. The dotted line was drawn by eye to pass through E_K, which was near 0 mV. Inset shows an amplitude histogram of 400 sec of data recorded at V_P of -130 mV. (*C*) Channel fluctuations elicited by a voltage ramp from a different cell than the one shown in (*A*). For all the recordings the pipette solution contained 140 mM K^+. The dotted line represents a linear fit to the single-channel currents during the ramp protocol.

sigmoid equation over the potential range studied (dotted line). The inflection point occurred at -120 mV. Maximum and minimum open probability were 87% at -80 mV and 47% at -150 mV, respectively.

Discussion

Our data show that in situ OLGs possess more types of ion channels than previously thought, and, in particular, for the first time we show the presence of delayed rectifying and inwardly rectifying K^+ channels in mature OLGs.

Morphology

LY-filled OLGs recorded in our study from P17–36 rats showed typical morphological features of mature OLGs in situ (Butt & Ransom, 1989; Bjartmar et al., 1994). OLGs had a mean process length of 132 μm, which is similar to that described by Butt & Ransom (1989) in rat optic nerve (150–200 μm) and longer than those of promyelinating OLGs recorded in mouse corpus callosum (60–70 μm) (Berger et al., 1991). This suggests that most of the recorded OLGs are close to their final length and have already established several myelin loops around axons. Recorded OLGs stained

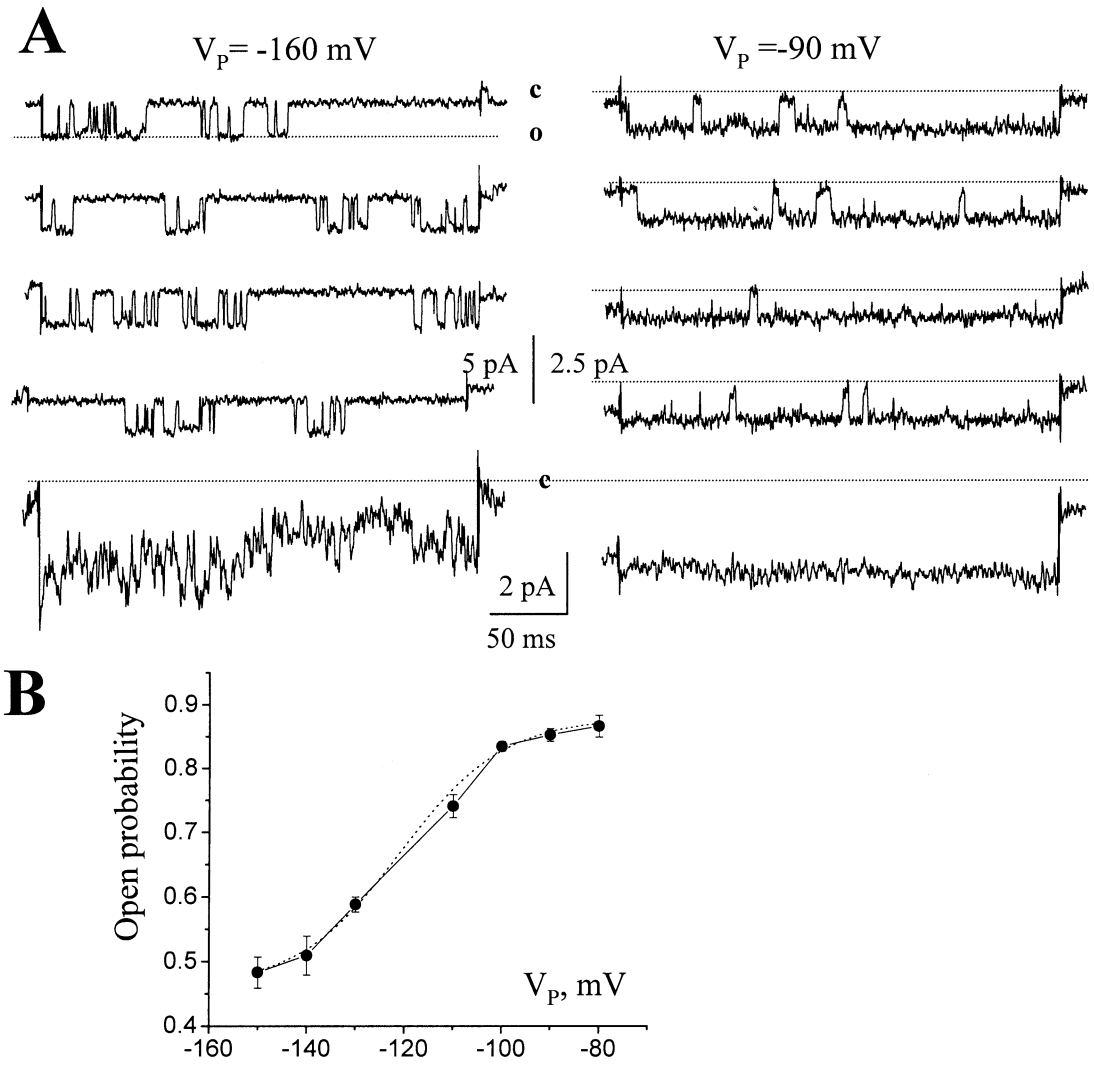

Fig. 6. Single-channel inactivation and open probability. (*A*) Cell-attached patch records of currents elicited in response to different voltage steps. The patch was held at a V_P of −75 mV (V_{PIP} = 0 mV and V_R = −75 mV) and stepped to −160 mV (left traces) and -90 mV (right traces). Beneath each group of sweeps is the averaged current record for that potential. 25–30 sweeps were applied with 3-sec intervals. Leak and capacitive currents recorded in response to equal and opposite steps were averaged and subtracted from each record. (*B*) Graph of open probability versus V_P. Records were 240 to 400 msec in duration and were obtained at different potentials applied in a random sequence.

positive for myelin basic protein that is synthesized only by mature OLGs. In addition, ensheathment of axons begins at P12 in rat corpus callosum and formation of compact myelin has clearly been initiated at P17 (Bjartmar et al., 1994). The mean number of ensheathed or myelinated axons was 15 (number of parallel processes; range 11 to 25), which was similar to the number of parallel processes previously reported in the corpus callosum (Bjartmar et al., 1994).

K^+ Channel Expression In Situ and Functional Implications

OLGs displayed voltage-dependent TEA-sensitive outward K^+ currents, Cs^+- and 100 μM Ba^{2+}-sensitive inward K^+ channels (K_{IR}) and 1 mM Ba^{2+}-sensitive K^+ currents.

Voltage-dependent K^+ Currents

Outwardly rectifying, non-inactivating currents were sensitive to TEA, activated between −50 and −40 mV, and resemble delayed rectifier currents present in mature OLGs in vitro (Barres et al., 1988; Soliven et al., 1988; Soliven et al., 1989; Attali et al., 1997). We observed outwardly rectifying K^+ currents in 78% of the recorded OLGs, which was more than in previous in situ reports (Berger et al., 1991; Chvatal et al., 1997). The reason for this discrepancy is not clear and might be due to technical differences, including, for instance, the amount of electrical cou-

pling and the intracellular medium used (amount of ATP, different pH). Interestingly, outward single-channel currents were not observed on the soma. This finding suggests that these channels are located on OLG processes as observed in Schwann cells (Mi et al., 1995), which could render their electrophysiological detection more difficult. This could also account for the small amplitudes of the TEA-sensitive currents that we recorded. Alternatively or additionally the small amplitudes of delayed rectifying K^+ channels in mature OLGs could be explained by the outward K^+ channel downregulation due to the switch from the progenitor proliferating phenotype to the post-mitotic myelinating phenotype (Attali et al., 1997; Chittajallu et al., 2002). In immature OLGs delayed rectifier K^+ channels have been shown to play a role in OLG proliferation/differentiation and myelination (Soliven et al., 1989; Attali et al., 1997; Chittajallu et al., 2002), while in mature OLGs their role remains elusive.

Inwardly Rectifying K^+ Currents

Our data show that mature OLGs express typical Cs^+- and 100 μM Ba^{2+}-sensitive inwardly rectifying K^+ channels, which is consistent with previous in vitro reports (Barres et al., 1988; Gaillard & Bossu, 1995; Attali et al., 1997) and in situ immunostaining of K_{IR} channel subunits in adult OLGs (Poopalasundaram et al., 2000). In addition, K_{IR} channels have been shown to be necessary for the maintenance of myelin (Soliven et al., 1994), which strongly suggests their presence in mature OLGs in situ (Neusch et al., 2000). The presence of K_{IR} channels was not investigated in previous in situ studies that either did not use pharmacological blockers (Chvatal et al., 1997) or used a higher Ba^{2+} concentration (10 mM) (Berger et al., 1991), which does not selectively block K_{IR} channels. Inwardly rectifying single-channel currents were observed in 75% of patches. These currents were carried by K^+ ions because the open and closed state of the single-channel currents intersect near 0 mV, which is close to the E_K (3–7 mV) and not close to the Nernst equilibrium potential of Cl^- ions (E_{Cl}). E_{Cl} was between +31 and +46 mV with a KGluconate-based pipette or between −44 and −58 mV with KCl (assuming an intracellular Cl^- concentration of 14–25 mM; Ballanyi, 1995; Stys et al., 1997). The mean single-channel conductance of 30 pS in 140 mM K^+ similar to that reported for K_{IR} channels in the rat optic nerve, whole brain bovine and human OLGs in vitro (Barres et al., 1988; McLarnon & Kim, 1989a; 1989b). Similarly, as previously reported, the open probability was voltage-dependent and K_{IR} channels were open 87% of the time at V_R. As reported for K_{IR} channels in bovine OLGs (McLarnon & Kim, 1989b), in our study, K_{IR} channels showed strong inward rectification but little inactivation at hyperpolarized potentials. Thus, K_{IR} channels in OLGs display the appropriate features to allow influx of K^+ into OLGs at rest. In addition, K_{IR} channels participate in the maintenance of V_R as shown by the ~13 mV shift in V_R after blocking K_{IR} channels.

Inward and Outward Time-dependent K^+ Currents

Mature OLGs display inward and outward time-dependent components of the whole-cell currents that are blocked by 1 mM Ba^{2+}. A similar effect using 10 mM Ba^{2+} was previously reported (Berger et al., 1991). In our study, voltage-independent K^+ channels significantly contributed to the establishment of the cell resting potential, as shown by positive shifts in V_R in the presence of 1 mM Ba^{2+}. This large K^+ permeability of the OLG membrane is likely important in the passive regulation of K^+ movement across the glial membrane, as previously suggested by Berger et al. (1991).

Overall, these data reconcile conflicting results obtained from previous in vitro and in situ studies on mature OLG ion-channel expression. In particular our findings show that mature oligodendrocytes in the corpus callosum do possess delayed rectifying K^+ channels and inwardly rectifying K^+ channels and that these latter channels participate in the maintenance of the cell resting membrane potential and are likely important for K^+ buffering in these cells.

We thank Dr. C. A. Greer for providing us with a scanning confocal microscope. This work was supported by NIH P01-NS39092-03.

References

Attali, B., Wang, N., Kolot, A., Sobko, A., Cherepanov, V., Soliven, B. 1997. Characterization of delayed rectifier Kv channels in oligodendrocytes and progenitor cells. *J. Neurosci.* **17:**8234–8245

Ballanyi, K. 1995. Modulation of glial potassium, sodium, and chloride activities by the extracellular milieu. In: Neuroglia, H. Kettenmann, and B.R. Ransom, editors. pp. 289–298. New York, Oxford University Press

Barres, B.A., Chun, L.L., Corey, D.P. 1988. Ion channel expression by white matter glia: I. Type 2 astrocytes and oligodendrocytes. *Glia* **1:**10–30

Berger, Z., Schnitzer, J., Kettenmann, H. 1991. Developmental changes in the membrane current pattern, K^+ buffer capacity, and morphology of glial cells in the corpus callosum slice. *J. Neurosci.* **11:**3008–3024

Bjartmar, C., Hildebrand, C., Loinder, K. 1994. Morphological heterogeneity of rat oligodendrocytes: electron microscopic studies on serial sections. *Glia* **11:**235–244

Bordey, A., Sontheimer, H. 1997. Postnatal development of ionic currents in rat hippocampal astrocytes in situ. *J. Neurophysiol.* **78:**461–477

Bordey, A., Sontheimer, H. 2000. Ion channel expression by astrocytes in situ: comparison of different CNS regions. *Glia* **30:**27–38

Butt, A.M., Colquhoun, K., Tutton, M., Berry, M. 1997. Three-dimensional morphology of astrocytes and oligodendrocytes in the intact mouse optic nerve. *J. Neurocytol.* **23:**469–485

Butt, A.M., Duncan, A., Hornby, M.F., Kirvell, S.L., Hunter, A., Levine, J.M., Berry, M. 1999. Cells expressing the NG2 antigen contact nodes of Ranvier in adult CNS white matter. *Glia* **26:**84–91

Butt, A.M., Ransom, B.R. 1989. Visualization of oligodendrocytes and astrocytes in the intact rat optic nerve by intracellular injection of lucifer yellow and horseradish peroxidase. *Glia* 2:470–475

Chittajallu, R., Chen, Y., Wang, H., Yuan, X., Ghiani, C.A., Heckman, T., McBain, C.J., Gallo, V. 2002. Regulation of Kvl subunit expression in oligodendrocyte progenitor cells and their role in G_1/S phase progression of the cell cycle. *Proc. Natl. Acad. Sci. USA* **99:**2350–2355

Chvatal, A., Anderova, M., Ziak, D., Sykova, E. 1999. Glial depolarization evokes a larger potassium accumulation around oligodendrocytes than around astrocytes in gray matter of rat spinal cord slices. *J. Neurosci. Res.* **56:**493–505

Chvatal, A., Berger, T., Vorisek, I., Orkand, R.K., Kettenmann, H., Sykova, E. 1997. Changes in glial K^+ currents with decreased extracellular volume in developing rat white matter. *J. Neurosci. Res.* **49:**98–106

Dawson, M.R., Levine, J.M., Reynolds, R. 2000. NG2-expressing cells in the central nervous system: Are they oligodendroglial progenitors? *J. Neurosci. Res.* **61:**471–479

Eng, L.F. 1985. Glial fibrillary acidic protein (GFAP): the major protein of glial intermediate filaments in differentiated astrocytes. *J. Neuroimmunol.* 8:203–214

Gaillard, S., Bossu, J.-L. 1995. Voltage-gated ionic currents in mature oligodendrocytes isolated from rat cerebellum. *Neurosci. Lett.* **190:**191–194

Hertz, L., Soliven, B., Hertz, E., Szuchet, S., Nelson, D.J. 1990. Channel-mediated and carrier-mediated uptake of K^+ into cultured ovine oligodendrocytes. *Glia* 3:550–557

Hida, H., Takeda, M., Soliven, B. 1998. Ceramide inhibits inwardly rectifying K^+ currents via a Ras- and Raf-1-dependent pathway in cultured oligodendrocytes. *J. Neurosci.* **18:**8712–8719

McLarnon, J.G., Kim, S.U. 1989a. Existence of inward potassium currents in adult human oligodendrocytes. *Neurosci. Lett.* **101:**107–112

McLarnon, J.G., Kim, S.U. 1989b. Single channel potassium currents in cultured adult bovine oligodendrocytes. *Glia* **2:**298–307

Mi, H., Deerink, T.J., Ellisman, M.H., Schwarz, T.L. 1995. Differential distribution of closely related potassium channels in rat Schwann cells. *J. Neurosci.* **15:**3761–3774

Neusch, C.A., Rozengurt, N., Lester, H.A., Kofuji, P. 2000. Failure of myelin formation and axonal degeneration in mice lacking the inwardly rectifying potassium channel KIR4.1 subunit. *Neurosci. Abstr. 401.***11:**1069

Newman, E.A. 1993. Inward-rectifying potassium channels in retinal (Muller) cells. *J. Neurosci.* **13:**3333–3345

Newman, E.A., Frambach, D.A., Odette, L.L. 1984. Control of extracellular potassium levels by retinal glial cell K^+ siphoning. *Science* **225:**1174–1175

Nishiyama, A., Chang, A., Trapp, B.D. 1999. NG2+ glial cells: a novel glial cell population in the adult brain, J. *Neuropathol. Exp. Neurol.* **58:**1113–1124

Orkand, R.K., Nicholls, J.G., Kuffler, S.W. 1966. Effect of nerve impulses on the membrane potential of glial cells in the central nervous system of amphibia. *J. Neurophysiol.* **29:**788–806

Petry, K.G., Boullerne, A.I., Pousset, F., Brochet, B., Caille, J.M., Dousset, V. 2000. Experimental allergic encephalomyelitis animal models for analyzing features of multiple sclerosis. *Pathol. Biol. (Paris)* **48:**47–53

Poopalasundaram, S., Knott, C., Shamotienko, O.G., Foran, P.G., Dolly, J.O., Ghiani, C.A., Gallo, V., Wilkin, G.P. 2000. Glial heterogeneity in expression of the inwardly rectifying K(+) channel, Kir4.1, in adult rat CNS. *Glia* **30:**362–372

Remahl, S., Hilderbrand, C. 1990. Relation between axons and oligodendroglial cells during initial myelination. I. The glial unit. *J. Neurocytol.* **19:**313–328

Simon, J.H., Holtas, S.L., Schiffer, R.B., Rudick, R.A., Herndon, R.M., Kido, D.K., Utz, R. 1986. Corpus callosum and subcallosal-periventricular lesions in multiple sclerosis: detection with MR. *Radiology* **160:**363–367

Soliven, B., Szuchet, S., Arnason, B.G.W., Nelson, D.J. 1988. Voltage-gated potassium currents in cultured ovine oligodendrocytes. *J. Neurosci.* **8:**2131–2141

Soliven, B., Szuchet, S., Arnason, B.G., Nelson, D.J. 1989. Expression and modulation of K^+ currents in oligodendrocytes: possible role in myelinogenesis. *Dev. Neurosci.* **11:**118–131

Soliven, B., Takeda, M., Szuchet, S. 1994. Depolarizing agents and tumor necrosis factor-α modulate protein phosphorylation in oligodendrocytes. *J. Neurosci. Res.* **38:**91–100

Soliven, B., Wang, N. 1995. Arachidonic acid inhibits potassium conductances in cultured rat oligodendrocytes. *Am. J. Physiol.* **269:**C341–C348

Sontheimer, H., Trotter, J., Schachner, M., Kettenmann, H. 1989. Channel expression correlates with differentiation stage during the development of oligodendrocytes from their precursor cells in culture. *Neuron* **2:**1135–1145

Sturrock, R.R. 1980. Myelination of the mouse corpus callosum. *Neuropathol. Appl. Neurobiol.* **6:**415–420

Stys, P.K., Lehning, E., Saubermann, A.J., LoPachin Jr., R.M., 1997. Intracellular concentrations of major ions in rat myelinated axons and glia: calculations based on electron probe X-ray microanalyses. *J. Neurochem.* **68:**1920–1928

Sutor, B., Schmolke, C., Teubner, B., Schirmer, C., Willecke, K. 2000. Myelination defects and neuronal hyperexcitability in the neocortex of connexin 32-deficient mice. *Cereb. Cortex* **10:**684–697

Williamson, A.V., Compston, D.A.S., Randall, A.D. 1997. Analysis of the ion channel complement of the rat oligodendrocyte progenitor in a commonly studied in vitro preparation. *Eur. J. Neurosci.* **9:**706–720